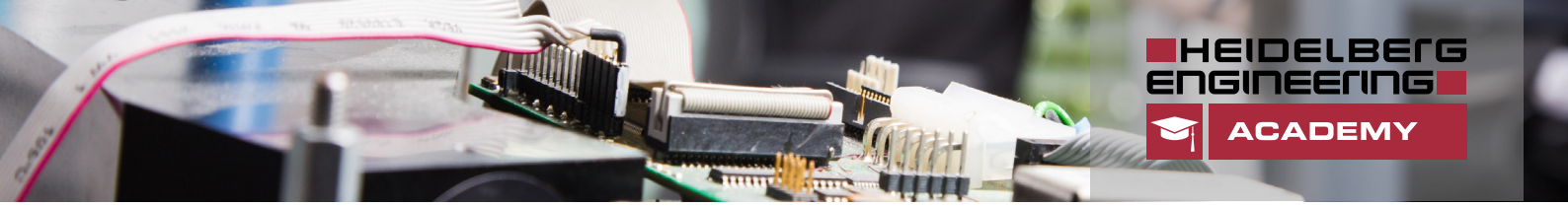

May 2019

State-of-the-art commercial Spectral-Domain and Swept-Source OCT technologies and their clinical applications in ophthalmology

Michel M. Teussink, PhD[1]; Sabine Donner, PhD[2]; Tilman Otto, PhD[3]; Krysten Williams[4]; Ali Tafreshi[1]

ABSTRACT

The commercial introduction of Swept-Source optical coherence tomography (SS-OCT) and its possible advantages relative to Spectral-Domain OCT (SD-OCT) has sparked the interest of eye care professionals. SS-OCT technology for imaging of the posterior segment has been suggested to offer additional clinical value relative to SD-OCT technology due to faster acquisition speed and optical penetration depth. It has also been proposed that long wavelength SS-OCT devices allow for the rendering of images with clinically significant advantages compared with those obtained using short wavelength SD-OCT devices.

This paper summarizes the relative strengths and limitations of both technologies, the significance of using a short wavelength versus long wavelength light source with each OCT technique, and the clinical implications of these technological combinations for imaging of the anterior and posterior segments of the eye.

A comprehensive description of current technological aspects of SD-OCT and SS-OCT sheds light on the rationale behind Heidelberg Engineering's decision to continue the development and optimization of SD-OCT technology for imaging of the posterior segment while adopting and optimizing SS-OCT technology for imaging of the anterior segment. With this approach, the advantages of each OCT technology have been capitalized on with the intent to offer eye care professionals optimal diagnostic imaging solutions for each indication.

BACKGROUND

Optical coherence tomography (OCT) has become the standard of care in the ophthalmic field and in many cases it serves as the technological workhorse for diagnostic imaging and management of various ocular conditions. The near-infrared light used in OCT readily penetrates media opacities to enable high-resolution, depth-resolved imaging of ocular structures that may be otherwise challenging to discern during an ophthalmoscopic examination.

The first generation of OCT technology is referred to as time-domain OCT (TD-OCT). TD-OCT acquires a depth scan at each location by an interferometric measurement of light echoes returning from the retina, measured relative to echoes returning from a reference mirror. By axially scanning this mirror, the reflectivity profile versus retinal depth is determined.[1]

Fourier-Domain OCT (FD-OCT) is the second generation of this technology,[2] with the first device becoming commercially available in 2006.[3] This technology simultaneously samples all retinal depths using a broad-spectrum light and a spectrometer, obviating the need to axially scan a reference mirror, while providing over a hundredfold improvement in speed and sensitivity.[4,5] An alternative approach to SD-OCT,[6–11] Swept-Source OCT (SS-OCT), was introduced shortly after, with the principle difference being the type of light source and detector. It is also based on spectral interference and, therefore, offers the same advantage in sensitivity over TD-OCT.[12] When SS-OCT technology was first introduced to the ophthalmic field, it presented with speed and optical depth penetration improvements relative to that of SD-OCT.

Corresponding author:

Sabine Donner, PhD

Heidelberg Engineering GmbH
Max-Jarecki-Straße 8
69115 Heidelberg

Retina@HeidelbergEngineering.com

[1] Product Management and Clinical Affairs, Heidelberg Engineering GmbH

[2] Research and Development, Heidelberg Engineering GmbH

[3] Technology Management, Heidelberg Engineering GmbH

[4] Academy, Heidelberg Engineering GmbH

The commercial introduction of SS-OCT in 2012[13] generated much interest among eye care professionals, because it offered the ability to acquire high-contrast, high-resolution images at about 4x higher acquisition speed as compared to commercial SD-OCT devices available at that time. SS-OCT devices showed less signal decay with depth and the use of longer imaging wavelengths resulted in deeper tissue penetration. However, since the inception of SS-OCT, SD-OCT technology has continued to advance quickly and significantly, keeping pace with the advantages offered with SS-OCT. These advancements have led to state-of-the-art SD-OCT and SS-OCT commercial devices with unique but similar technical and clinical performance. For example, the fastest currently available commercial OCT device uses SD-OCT technology (250k A-scans/s).[14]

Misinformation has led to confusion regarding the different technical properties of OCT in general, the state-of-the-art of SD-OCT and SS-OCT devices and their relative technical performance, the evidence of clinically significant advantages of one over the other, and of the potential of future advancements for each technology. Heidelberg Engineering (HE) has invested early and significantly in both technologies, carefully assessing their relative technical and clinical benefits as well as limitations in various ophthalmic applications.

This document summarizes and highlights the rationale behind Heidelberg Engineering's decision to continue the development of the SPECTRALIS® SD-OCT platform for imaging of the posterior ocular segment and the current development of an SS-OCT platform for imaging of the anterior segment. In doing so, the technical properties of each approach are summarized and their implications on clinical utility are highlighted.

THE EVOLUTION OF OCT TECHNOLOGY

OCT technology is often compared to Medical Ultrasound imaging since both imaging modalities direct waves to a specified tissue. The echo of the back-reflected waves from each tissue is analyzed in order to reveal the depth of the back-reflection. Analyzing the intensity of these backreflected waves reveals the strength of the reflector. The main difference between Ultrasound and OCT is that the latter uses light waves instead of sound waves. The shorter wavelength of light compared to longer ultrasound waves allows for OCT images to have significantly better resolution.

Light travels much faster than sound and, therefore, the delays of the reflected waves cannot be measured directly. Instead, light coming from a low coherent light source is split: one part is directed to the sample and another is directed to a reference beam path with a known length. As the light returns from the individual paths (one known, the other one under investigation), it is combined and the interference patterns reveal the optical delay and the strength of back-reflection. This measurement is referred to as low coherence interferometry. One interferometric measurement forms one reflectivity profile of the tissue along a depth: the so-called A-scan. Scanning the beam laterally across the sample forms cross-sectional images referred to as brightness scans (B-scans). The term B-scan has been adopted from Medical Ultrasound, emphasizing the similarity of the two technologies again.

The OCT variants that have been developed are different implementations of this interferometric detection method. The first implementation of OCT technology was TD-OCT. Due to the low coherence length of the light source, the light from the sample arm and from the reference arm only interferes when the arm lengths match within the coherence length of the light source.[1] TD-OCT is relatively straightforward: the reference mirror is scanned along the depth range and a photodiode is read out at each depth location. Plotting the photodiode readout along depth directly generates the A-scan. However, the required depth scanning makes TD-OCT slow, with a poor sensitivity compared to subsequent OCT technologies.

In the second generation of OCT technology, Fourier-Domain OCT (FD-OCT),[2,15,16] time delays are measured indirectly based on the spatial modulations of the spectrally resolved interference spectrum. These modulations are called fringe frequencies, where high fringe frequencies encode great arm length differences and, therefore, greater sample depth. By Fourier-transformation of the interference spectrum, the strength of reflections versus sample depth can be determined – without the need to move the reference mirror. The ability to capture the whole depth profile of one location in one shot allows FD-OCT technology to significantly improve acquisition speed, contrast,[4,5] and axial resolution[17,18] compared to TD-OCT.

The following section will compare the two Fourier-Domain OCT technologies, SS-OCT and SD-OCT, with a focus on factors and physical concepts needed to understand the similarities and differences relevant to ophthalmic images.

1.1 Spectral-Domain OCT and Swept-Source OCT

The main components of an FD-OCT system are depicted in **Figure 1**, including the key technical differences between SD- and SS-OCT systems. For both technologies, the light source emits a broad wavelength range called its spectrum. The spectrum is centered at a wavelength and the range is referred to as the spectral width. The light is then directed to an interferometer, which has the same main components for both SD- and SS-OCT systems. At the beam splitter, the light is split into a reference arm and a sample arm. The reference arm consists of a reflector at a known distance whereas in the sample arm the light is deflected by a scanner to allow for lateral sampling. An objective lens then focuses the beam onto the sample. After back-reflection from the sample and the reference arm, the light is recombined at the beam splitter and leaves the interferometer. The detector samples the combined light wavelength-by-wavelength to record the interference spectrum. The fringes on the spectrum (see **Figure 1**) carry the image information

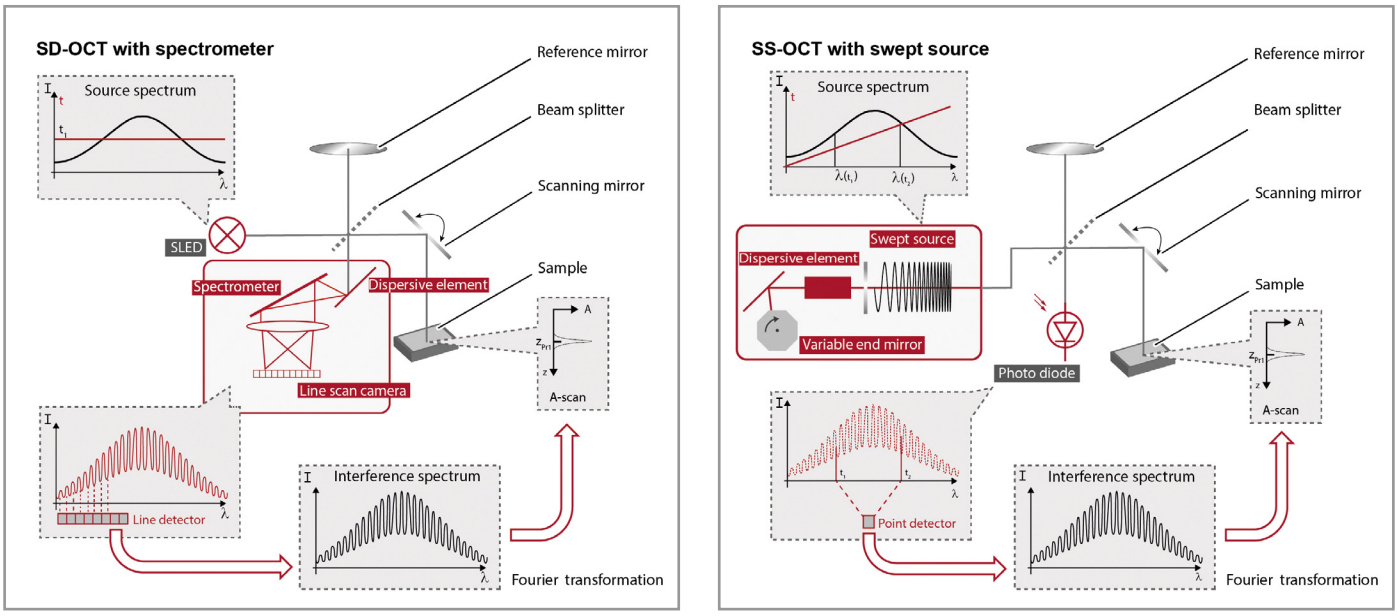

Figure 1. *The setup of Spectral-Domain OCT (left pane) and Swept-Source OCT (right pane) mainly differs with respect to the light source and detector. Other core elements needed for OCT, including the interferometer, scanning, and focusing optics can be the same.*

as their frequency decodes the depth in which the reflection took place. These frequencies are analyzed by Fourier transformation to convert the spectral information into an A-scan.

SD-OCT uses a superluminescent diode as its light source that simultaneously emits all wavelengths; and, therefore, the detector is required to apply wavelength-separation. Separation into narrow portions of the interference spectrum is done by a dispersive element; the light rays are then focused on a line-scan camera, enabling simultaneous recording of all wavelengths. Once enough light has been detected at one location in the sample to generate an A-scan, the OCT beam can be steered to the next location and the process repeats to generate a series of A-scans that create a B-scan.

In SS-OCT, a laser is used which sequentially emits narrow portions of the source spectrum synchronously with a high-speed point sensor. Once the laser has emitted the whole spectrum, a sweep is completed and an A-scan is generated. From this point on, both techniques are identical in principle again as the B-scan is formed by steering the beam to the next position along the scan path and stringing together the A-scans.

1.2 Signal-to-Noise Ratio and Sensitivity

Contrast defines how well structures can be distinguished within cross-sectional images. In OCT, certain system parameters contribute to the visibility of structures: signal-to-noise ratio (SNR) of structures, sensitivity of the OCT system and sensitivity decay with depth, often referred to as roll-off. As depicted in **Figure 2** for an exemplary A-scan, SNR is the distance of a signal from the noise floor and it can be directly appreciated in OCT B-scans as contrast of structures. This signal height in the A-scans is transferred into grey values to generate the B-scans. However, as this signal height is highly dependent on the reflectivity of the structure, SNR cannot be interpreted independently from sample properties.

Sensitivity is a standardized measure for performance of an OCT-system, independent from sample characteristics. As shown in **Figure 2**, the sensitivity is the signal height in an OCT A-scan that would be generated if the sample was an ideal mirror. A system with a higher sensitivity would be able to generate a better signal from a sample that is being measured. This means that the sensitivity of an OCT system describes the weakest detectable signal above the noise floor. There is sensitivity decay with depth (also shown in **Figure 2**), meaning that the SNR drops and the system loses its ability to detect the weakest signals with increasing depth.

The sensitivity of an OCT system is increased by lowering the noise floor and/or by optimizing the signal strength. The noise floor and the detection efficiency are both determined by the detector, which are different in SS- and SD-OCT systems. Both techniques can achieve equal sensitivity of more than 100 dB.[12]

Another parameter that directly impacts signal strength is integration time: the longer the integration time for one A-scan, the higher the sensitivity. As integration time is the time period during which one A-scan is captured, it is inversely related to acquisition rate and there is a trade-off between sensitivity and acquisition speed. Increasing the A-scan rate by a factor of 2 leads to a 50% loss of integration time and therefore to a 50% loss of sensitivity, which translates to 3 dB in the conventional sensitivity units.

The development of the SPECTRALIS OCT2 Module by Heidelberg Engineering took advantage of the significant improvement of line scan cameras that has taken place since the introduction of SD-OCT technology. The line scan camera implemented in the OCT2 spectrometer has twice the A-scan rate and increased quantum efficiency compared with that implemented in the first

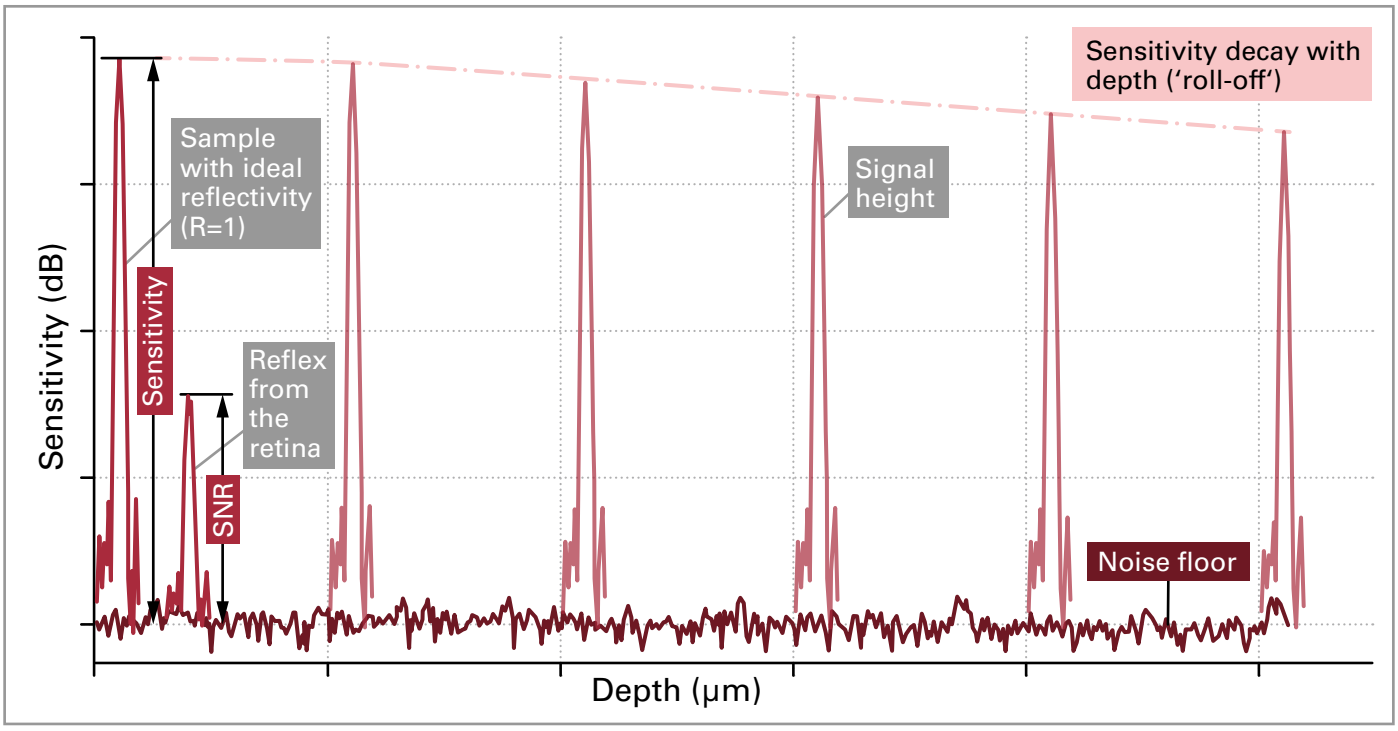

Figure 2. *Schematic of OCT contrast measures.*

SPECTRALIS OCT spectrometer. Despite the lower integration time due to the faster acquisition speed, the enhanced line scan camera and spectrometer provide a sensitivity improvement of approximately 2 dB for the OCT2 system relative to the original OCT system.

The signal strength can also be improved by raising the output power of the source. An OCT system with a higher source power will have a higher sensitivity. However, the increase in source power does not necessarily result in better SNR and tissue contrast for retinal imaging. As stated in the previous section, SNR is determined by the signal of a specific sample, how much light reaches the sample, how much light is reflected, and how much this light is attenuated before reaching the detector.

In order to compare the impact of laser power on SNR, the maximum exposure limits defined by laser safety guidelines are calculated. These exposure limits are calculated assuming a steady beam operation in the following example. At 850 nm, the maximum allowed output power is 0.73 mW, whereas it is 1.90 mW at 1050 nm center wavelength. Although a system that utilizes more laser power offers the potential for higher sensitivity, most of the benefit for SNR of the retinal structures is mitigated by water absorption. The overall signal attenuation, estimated based on an eye length of 24 mm and the assumption of only water absorption, is plotted in **Figure 3**. The center wavelengths of SD-OCT (solid red) and SS-OCT (solid grey) are illustrated. For this example calculation, the power at 850 nm is reduced to 0.62 mW and for 1050 nm to 1.03 mW, when only water attenuation is accounted for (assuming 100% reflection of all laser power). This

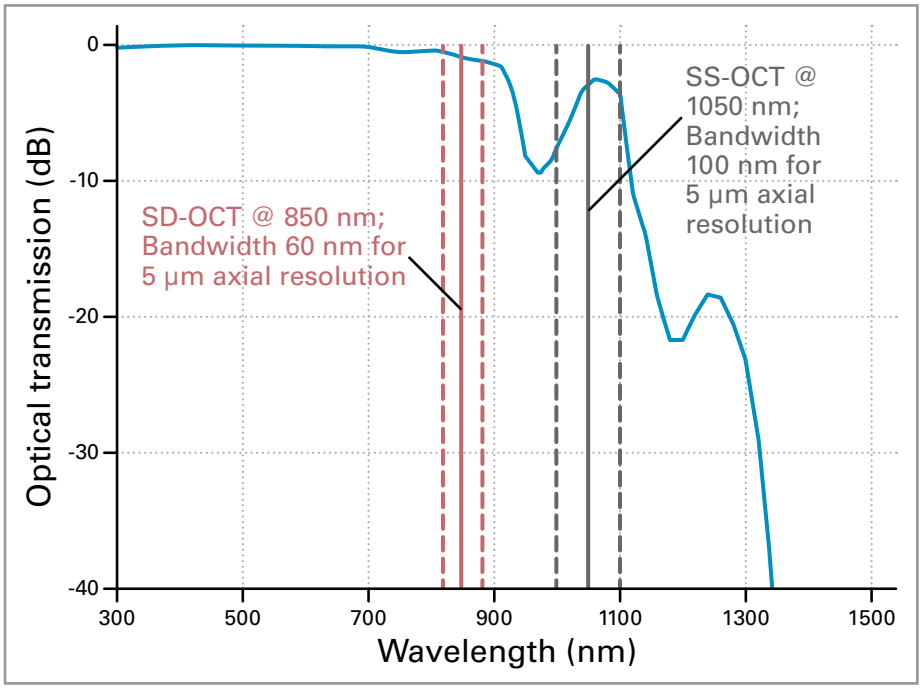

Figure 3. *Attenuation of light in OCT by water absorption in the eye (blue line), estimated based on an eye length of 24 mm and the assumption of only water absorption. Center wavelength (solid straight lines) for typical SD-OCT systems at 850 nm (in red) and SS-OCT systems at 1050 nm (in grey) are indicated. The dashed lines demarcate the spectral bandwidths for the two wavelength settings which are needed to achieve 5 µm axial resolution. Even though both ranges avoid the strongest water absorption bands at ~1000 nm and 1100 nm, the light attenuation is greater for 1050 nm, compared to 850 nm.*

indicates that the gain in signal from this longer wavelength cannot be higher than a factor of 1.7, despite a nearly three-fold higher input power at the maximum safety limits.

In the anterior segment, absorption is negligible because the optical path through water is shorter. Therefore, SS-OCT technology combined with a longer wavelength light source even beyond 1050 nm offers significant advantages for anterior segment imaging: higher laser power increases sensitivity and allows for a higher penetration depth into the tissue.

Acquiring multiple B-scans at the same location and averaging them enhances the SNR and improves the ability to discern anatomic details. B-scan averaging increases sensitivity by increasing the effective integration time at one location.

Speckle is the intensity pattern that forms due to the interferometric detection method. The acquisition of multiple B-scans at the same location requires accurate tracking of involuntary eye motion. Eye tracking causes the same location to be scanned with a different optical path, altering the speckle pattern. The above mentioned averaging of B-scans allows for speckle to be significantly reduced while the signal from structures is preserved. The SPECTRALIS confocal scanning laser ophthalmoscope (cSLO) enables realtime eye tracking and OCT image averaging by serving as the foundation for eye motion tracking during acquisition of multiple B-scans (see section *1.5 Techniques to Enhance Image Contrast and Signal-to-Noise Ratio*).

1.3 Image Depth Range and Signal Roll-Off

The depth range is the axial extent of an A-scan and it, therefore, determines the depth range covered by a B-scan. In OCT technology, the depth of a scattering structure is measured by analyzing the fringe frequency of the interference spectrum. Higher fringe frequencies are generated at greater depths. In EDI-mode, the inverse relation is true; i.e. lower fringe frequencies are generated at greater depths. The maximum detectable fringe frequency is called the spectral resolution. The maximum sampling depth, and therefore the OCT depth range, is determined by this maximum fringe frequency.

In SD-OCT, the light-source emits the full spectrum simultaneously and the spectrometer separates and detects the spectral information. At a dispersive element, the spectrum is first split into locally separated wavelength portions which are focused onto a line scan camera with a finite number of pixels. The number of pixels determines the spectral resolution and thereby the maximum depth range for SD-OCT systems. In practice, the wavelengths cannot be mapped ideally onto one single pixel. Limitations of the focusing optics and electronic noise of the line scan camera cause leakage of signal intensity to neighboring pixels. This effect lowers the sensitivity for higher frequencies and results in the sensitivity decay with depth.

The SPECTRALIS OCT2 Module employs a line scan camera with twice as many pixels than that implemented in the original SPECTRALIS OCT, with further enhanced focusing optics within the spectrometer. Therefore, the OCT2 Module is able to cover twice the depth range of the original SPECTRALIS OCT with the same sampling in depth (µm/pix in the depth dimension). To keep the depth range equal to the original SPECTRALIS OCT (~2 mm), only the upper half of the axial imaging range is used. Within this depth range, the roll-off of the system improved by up to 10 dB, as shown in **Figure 4**. These modifications ensure data compatibility and integrity between the two set ups and hence the ability to continue longitudinal data analysis, including comparability to the reference databases acquired using the original SPECTRALIS OCT system.

Sensitivity defines the starting point of the roll-off curves. As can be seen in **Figure 4**, the sensitivity for OCT2 is about 2 dB higher compared to the original OCT. The SNR curves of OCT and OCT2 represent measured data, showing that the sensitivity roll-off is significantly smaller for OCT2. This results in more than 10 dB gain in SNR at the greatest imaging depth of 1.92 mm.

In SS-OCT technology, the spectral resolution is given by the instantaneous line-width of the light source. One sweep can be described as a series of single wavelength lines where one readout of the photodiode is required for each wavelength. This time-sequenced readout allows for separation of the lines, resulting in low sensitivity decays for SS-OCT. In order to compare the signal roll-off of an SS-OCT system with that of the SPECTRALIS OCT2 Module, the roll-off curve of a theoretical SS-OCT system has been calculated from a paper specifying the roll-off of an experimental SS-OCT system with -2.4 dB/mm[19] (**Figure 4**). The sensitivity of the system was not stated and, therefore, it was set to be one dB higher than that of the OCT2 Module. The error band indicates the uncertainty of

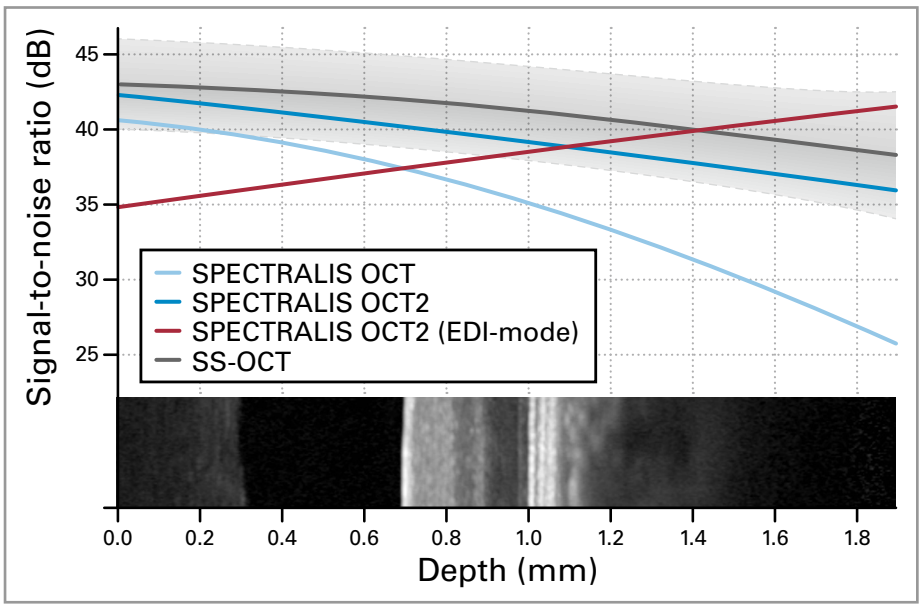

Figure 4. *Roll-off curves for SPECTRALIS OCT and OCT2 in comparison to a hypothetical SS-OCT device. Within the depth range of the retina, illustrated by the B-scan, the sensitivity difference between the OCT2 in standard mode and an SS-OCT system is negligible. OCT2 EDI-mode allows for even higher sensitivity for the deeper imaging range.*

the SS-OCT system properties. It can be appreciated that for the depth range of 2 mm, the roll-off of the OCT2 Module is parallel to the SS-OCT roll-off, suggesting that the SS-OCT system does not provide a signal roll-off advantage within the considered depth range.

The OCT B-scan depicted in **Figure 4** illustrates that within the depth range of the retina, the sensitivity differences between the OCT 2 and SS-OCT systems are negligible. To mitigate the signal roll-off effect that may impact visibility of the deeper ocular structures, the SPECTRALIS OCT offers the enhanced depth imaging (EDI) mode. The EDI mode shifts the imaging reference plane in order to ensure that the highest sensitivity is achieved at the maximum sampling depth. EDI results in the inversion of the signal roll-off curve, allowing for enhancement of SNR for deeper ocular structures (**Figure 4**).

1.4 Axial Resolution

Axial resolution is defined as the minimal distance at which two scattering objects within a sample can be separately detected along the A-scan (in depth).

Because of the interferometric measurement principle of OCT, the axial resolution is only dependent on the light source which is used for imaging. The focusing ability of the sampling beam does not define the axial resolution. This is a unique property of OCT technology, which enables very high axial resolution despite the low numerical aperture (NA) of the eye, a limiting factor for axial resolution in confocal microscopy.

Axial resolution is determined by the coherence length of the light source, which is defined by the center wavelength squared divided by the spectral width (or bandwidth). This means that a higher axial resolution can be achieved by using a broader spectrum of the light source. On the other hand, the linear dependency of the center wavelength means that for light sources with longer wavelengths more bandwidth is needed to achieve the same resolution. For example, to achieve an axial resolution of 5 µm (typical range of commercial OCT devices: 4 µm – 8 µm), a SD-OCT device at 800 nm needs a bandwidth of 60 nm, whereas a SS-OCT device at 1050 nm center wavelength needs a bandwidth of 100 nm to achieve the same axial resolution.

To further improve axial resolution at a given center wavelength, a light source with a broader bandwidth is necessary. A broader bandwidth of the light source requires a detector that provides sufficient sampling to maintain imaging depth (see section *1.3 Image Depth Range and Signal Roll-Off*). The limited availability and high costs of broader bandwidth light sources and detectors with sufficient sampling have set the resolution limits of

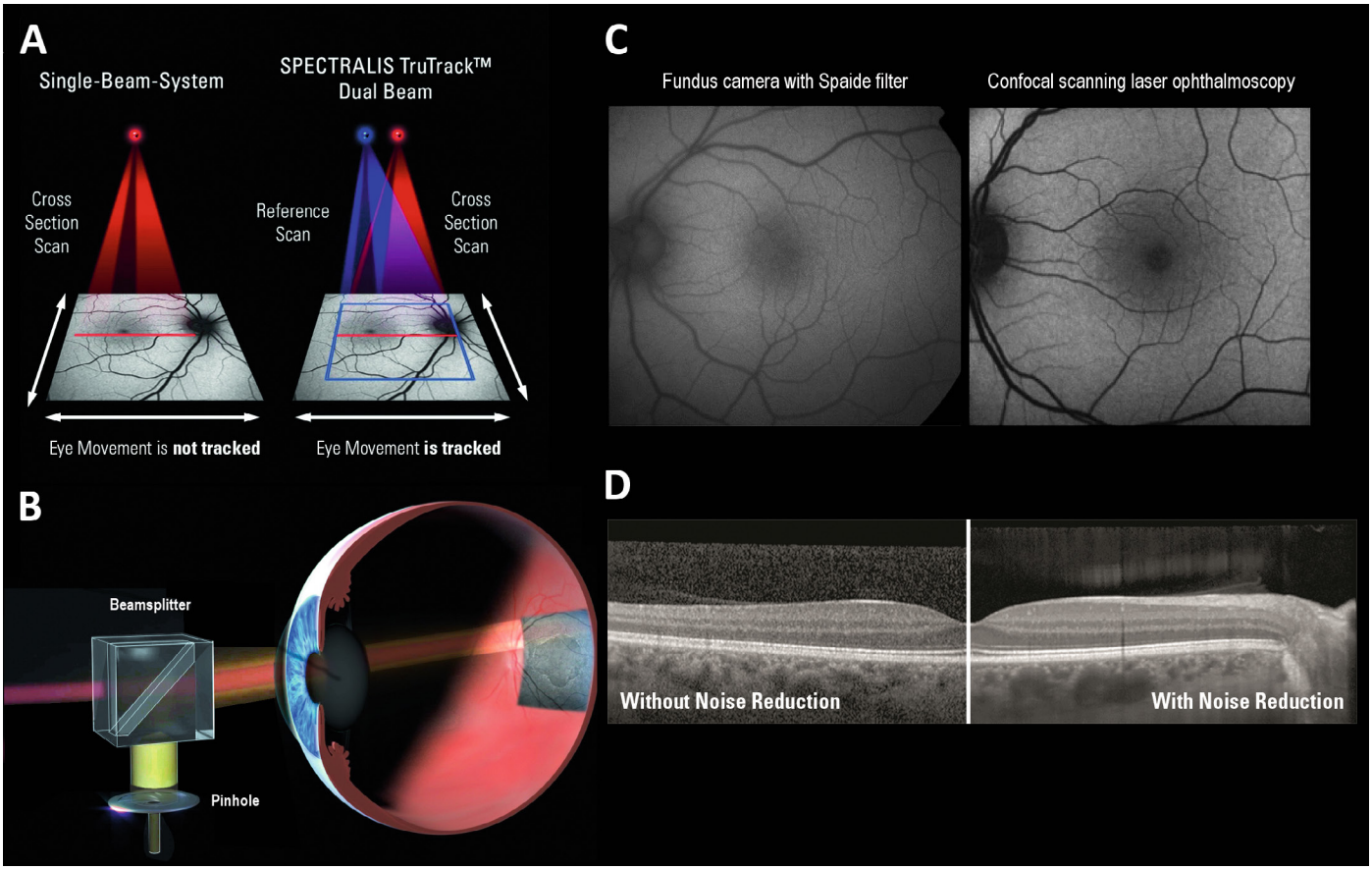

Figure 5. *Core DNA of SPECTRALIS.* ***(A)*** *TruTrack is a dual-beam tracking system which provides very important clinical benefits such as retinal recognition, follow-up scanning, image averaging to improve image quality, and precise co-localization of fundus images with depth-resolved information in OCT scans.* ***(B)*** *Confocal scanning laser ophthalmoscopy (cSLO) ensures that light reflected off the sample is filtered through a pinhole aperture, ensuring the rejection of stray light outside of the focal plane and thereby greatly increasing image quality and contrast.* ***(C)*** *Image comparison of a fundus autofluorescence image with a fundus camera modified with a Spaide filter (left) and with cSLO technology (right).* ***(D)*** *Multiple images, such as OCT B-scans, can be acquired at the same location using TruTrack, which allows for real-time image averaging to highly reduce noise and increase image quality.*

commercially available OCT devices. Another limitation of increasing axial resolution is directly related to the optical properties of the ocular media. The attenuation curve of water is shown in **Figure 3** where the center wavelength and the spectral bandwidth of OCT systems with 5 µm axial resolution are indicated. The red range marks an SD-OCT at 850 nm, indicating the potential to extend the bandwidth towards shorter wavelengths and, therefore, improving axial resolution without suffering from attenuation that long wavelength SS-OCT light sources do within their currently used bandwidths (marked in grey). Even if increasing the bandwidth for the 1050 nm light sources might technically be possible, the significantly increased absorption below 1000 nm and above 1100 nm by the ocular media hinders effective axial resolution gain.

1.5 Techniques to Enhance Image Contrast and Signal-to-Noise-Ratio

As mentioned earlier, the interferometric measurement technique used in OCT technology is prone to speckle noise in the images that are derived from it. There are no principle differences in speckle generation or speckle size between SD-OCT and SS-OCT systems and the intensity of speckles is not related to the technical characteristics of the hardware used in OCT devices. Due to the random nature of speckle noise, averaging of multiple image acquisitions over the same tissue suppresses the noise, as the speckle pattern changes between repeated B-scans. In order to achieve an effective level of noise suppression across multiple OCT B-scans and across a volume of data, high-speed and precise tracking of ocular motion is necessary (**Figure 5**).

Although some commercially available SD-OCT and SS-OCT devices offer eye tracking technology, only a few offer real-time image averaging for OCT volume scans. To accurately and precisely track the fundus, monitor ocular motion, and place multiple scans on the same location in order to achieve real-time image averaging, SPECTRALIS employs high-contrast and high-resolution confocal scanning laser ophthalmoscopy (cSLO) – an imaging technique which ensures that only light coming from the focal plane enters the detector while rejecting intraocular stray light, by using a pinhole aperture (**Figure 5b**). The result is a confocal image with greatly enhanced contrast of the fundus as compared to fundus photography (**Figure 5c**). The cSLO imaging modalities offered on SPECTRALIS range from fluorescein angiography, indocyanine green angiography, MultiColor, BluePeak, and near-infrared reflectance.

The near-infrared reflectance images are acquired continuously and separately from the other modalities available on the SPECTRALIS platform. Displacements or torsional motion of the retina relative to the scanning start position will be reflected in the individual near-infrared frames. A 'freeze capture' at the retinal location of interest is achieved by calculating this motion and compensating for it in real time by re-steering of the second imaging beam. This core feature of SPECTRALIS is called TruTrack Active Eye Tracking (**Figure 5a**).

The integration of eye tracking, image averaging and, therefore, increased image quality in general, and the combination of cSLO imaging with SD-OCT on the SPECTRALIS multimodal imaging platform, provide very important clinical benefits compared to OCT devices that do not offer these functionalities. Current commercial SS-OCT devices do not employ cSLO imaging. SPECTRALIS employs TruTrack Active Eye Tracking to enhance the image quality of all of its imaging modalities – including cSLO and OCT – to reduce the random noise by Automatic Real-Time averaging (**Figure 5d**). Depending on the desired level of noise reduction, the number of images averaged can be modified in order to achieve sufficient image quality. The more each image is averaged, the higher the level of noise suppression.

CLINICAL IMPLICATIONS OF SHORT WAVELENGTH SD-OCT AND LONG WAVELENGTH SS-OCT TECHNOLOGIES

In the clinical setting, the specific differences between SD-OCT and SS-OCT relate to tissue contrast, resolution to discern different anatomical structures, or a combination of both aspects. Another clinically relevant aspect is the depth range of OCT images (see section *1.3 Image Depth Range and Signal Roll-Off*).

1.6 Visibility of the Vitreous and Vitreoretinal Interface

The impact of long wavelength versus short wavelength light sources on the ability of OCT devices to visualize the vitreous and vitreoretinal interface has also been investigated. One study used an SD-OCT device equipped with both a short wavelength and long wavelength light source to conclude that the short wavelength images provided better contrast of the vitreoretinal interface while the long wavelength images showed better contrast of the choroid.[20] Vitreomacular traction was much less visible on the long wavelength OCT images.[20] These results were corroborated by another study which employed a 'full-depth imaging' technique for SD-OCT (i.e. OCT capture after a slight focus shift to positive value to highlight the vitreous, followed by OCT capture in EDI-mode, and combining the result with ART-mode) (**Figure 6**).[21] Various methods have been developed to enhance the lower intrinsic vitreous contrast using SS-OCT devices with longer wavelengths.[22–24] One such method has been implemented in a commercial SS-OCT and is referred to as "Enhanced Vitreous Visualization" (EVV).

A few studies have concluded that this software feature leads to better visualization of the bursa pre-macularis, or the posterior pre-cortical vitreous pockets (PPVP, which are often mistaken for posterior vitreous detachment using non-averaged OCT scans), the Martegiani space, Clocquet's canal, posterior cortical vitreous, posterior hyaloid, and vitreous opacities of different etiologies.[25–27] To date, software-based methods to enhance vitreous contrast have not been implemented in commercial SD-OCT devices as the

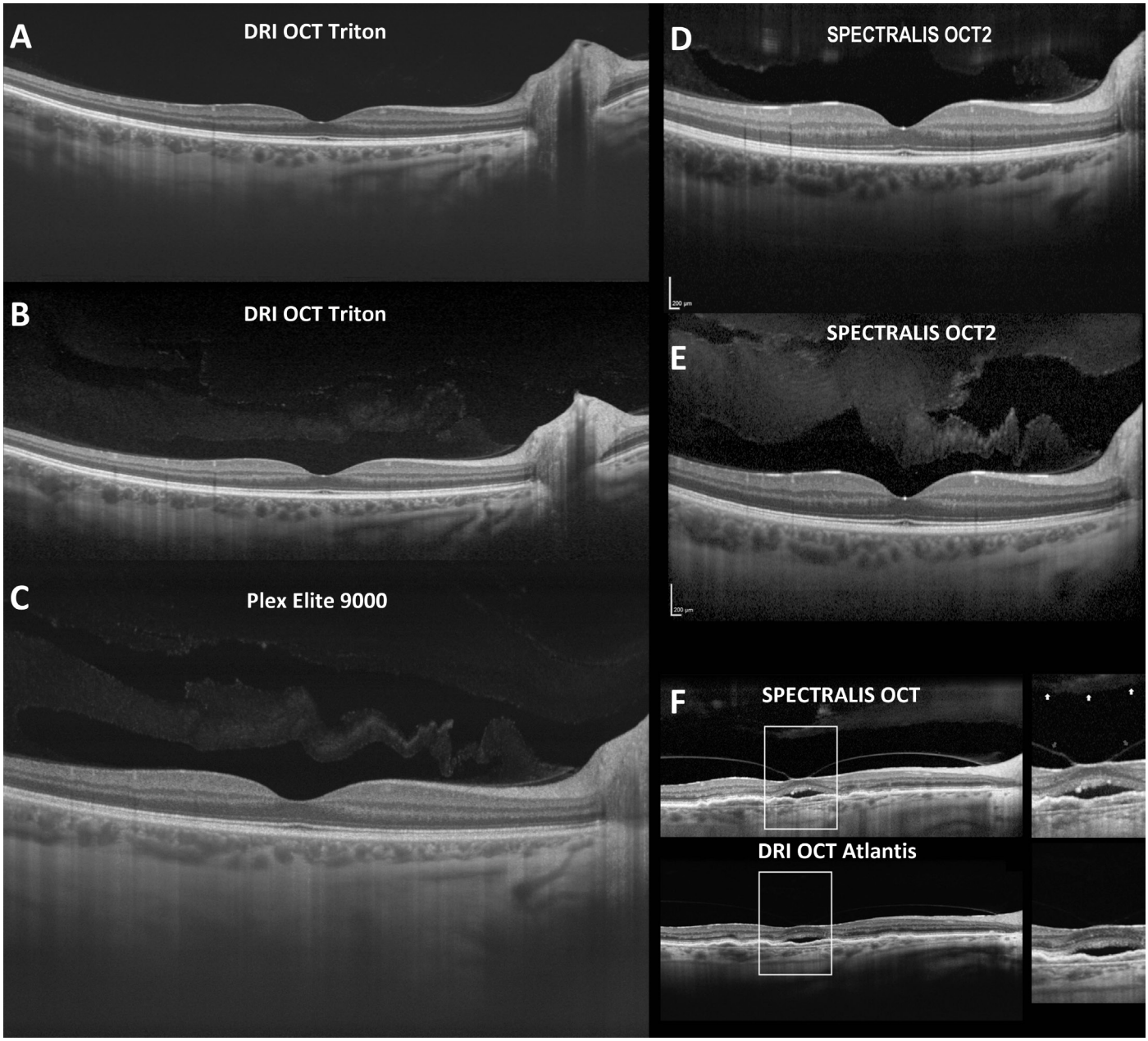

Figure 6. *Visibility of the vitreous and vitreoretinal interface with SD-OCT and SS-OCT, using various techniques to enhance vitreous contrast.* ***(A)*** *Averaged B-scan (n=128) using the DRI OCT Triton SS-OCT device.* ***(B)*** *DRI OCT Triton SS-OCT B-scan with Dynamic Focusing and Enhanced Vitreous Visualization.* ***(C)*** *Averaged B-scan (n=100) using the Plex Elite 9000 SS-OCT device.* ***(D)*** *Averaged B-scan (ART=100) using the SPECTRALIS SD-OCT with OCT2 Module.* ***(E)*** *SPECTRALIS SD-OCT with OCT2 Module B-scan acquired using Full-Depth Imaging protocol.* ***(F)*** *Image comparison in a case with vitreoretinal traction,[21] showing SPECTRALIS OCT without OCT2 Module and Full-Depth Imaging protocol (top) with magnified Inset (right), and averaged B-scan taken with Topcon DRI OCT Atlantis SS-OCT (bottom) with magnified inset (bottom right). The image comparisons in* ***(F)*** *show that the intrinsic vitreoretinal contrast using the longer wavelength SS-OCT device is lower and insufficient to detect the vitreoretinal traction.[21]*
Image courtesy of Prof. Giovanni Staurenghi and Mariano Cozzi, Department of Biomedical and Clinical Science "Luigi Sacco", University of Milan, Italy.

images provide better intrinsic vitreous contrast due to their shorter wavelength.

1.7 Visibility of Retinal Structures

Eye care professionals heavily depend on automated segmentation of retinal layers that provide the measurement parameters used to make clinically relevant decisions. These parameters are typically used to diagnose and manage diseases such as diabetic macular edema, retinal vein occlusion, glaucoma, and/or other optic neuropathies. The reliable segmentation of all retinal layers also determines the reliability and subsequent clinical validity of OCT Angiography (OCTA) images. OCTA images heavily depend on the correct segmentation of certain retinal boundaries in order to generate anatomically accurate en face renditions of different retinal vascular plexuses.

Several studies have investigated the use of long wavelength OCT devices versus short wavelength OCT devices and their ability to generate clinically relevant retinal thickness measurements. Circumpapillary retinal nerve fiber layer (cpRNFL) thickness measurements are commonly relied upon metrics for glaucoma diagnosis and management. While the cpRNFL parameter of long wavelength OCT and short wavelength OCT devices has

been shown to be similar in repeatability[28] and glaucoma discriminatory ability,[29–32] there are significant differences between these devices' abilities when using macular inner retinal layer parameters.[29,31] These macular measurements have been shown to be diagnostically specific and sensitive at discriminating between healthy eyes and those with glaucoma,[31,32] with the short wavelength OCT providing overall more repeatable and reproducible results compared to long wavelength OCT.[33]

Within the inner plexiform layer (IPL), bipolar cells (the first order neurons of the visual pathway) connect to the dendrites of the retinal ganglion cells (RGCs), the second order neurons of the visual pathway. The RGC cell bodies lie within the ganglion cell layer (GCL). Mechanical damage to RGC axons may lead to disruption of axonal transport of molecules that are essential for the survival of these cells during early stages in the pathogenesis of glaucoma.[34] Fewer structural variations of the GCL have been hypothesized to exist in the normal population than RNFL variations.[35] Therefore, the ability to segment the GCL on the standard SPECTRALIS viewing software[36,37] or on third party software[38] may lead to a reliable metric that serves as an aid to the early diagnosis of glaucoma.

In addition, evidence suggests that in early glaucoma, architectural changes in the dendrites (in the IPL) are followed by RGC death.[39] Since about 50% of the RGCs lie within a 16° circle centered on the fovea,[40] it may be clinically important to include an assessment of macular structures in the OCT-based management of glaucoma [40,41] by separating the IPL, GCL, and macular NFL.[42] The short wavelength OCT light source allows for better contrast between retinal layers as compared with a long wavelength light source. This characteristic combined with enhanced OCT image quality provided by TruTrack Active Eye Tracking optimizes the ability to discern the IPL, GCL,and RNFL. The differences in the intrinsic retinal contrast between short wavelength SD-OCT and longwavelength SS-OCT, and the impact of eye tracking, are explained in detail below in section *1.10 Short Wavelength SD-OCT and Active Eye Tracking*.

It is important not to overlook the importance of data compatibility for the longitudinal monitoring of patients with glaucoma. Thickness measurements obtained with different OCT devices cannot be used interchangeably due to fixed and relative biases, mainly caused by the use of light sources with different center wavelengths, but also due to potentially different segmentation algorithms.[28,30,33] As both the original OCT platform and the OCT2 Module of the SPECTRALIS use the same light source and segmentation algorithm, data compatibility is ensured.

Reduced scattering by long wavelength OCT imaging should result in better penetration of cataracts as compared to short wavelength OCT imaging, which in this case results in images of the posterior ocular segment with higher SNR.[43] Long wavelength OCT macular imaging of gas-filled eyes after vitrectomy allows for sufficient visibility of retinal structures more frequently than imaging done on short wavelength OCT imaging, i.e. the ability to sufficiently visualize retinal structures allows for the evaluation of surgical success in patients with macular holes or retinal detachments in the early post-operative period.[44] This difference is caused by increased optical scattering when using short wavelength light at the air-fluid interface, leading to a greatly reduced OCT signal at the retina. In rare instances, long wavelength OCT imaging offers the potential to better visualize retinal structures when compared with short wavelength OCT imaging but the overall retinal contrast of these images is poor on both wavelengths.

1.8 Visibility of the Choroid and the Sclera: Short Wavelength OCT vs. Long Wavelength OCT

In optical imaging, the greatest depth at which distinct features can be discerned is determined by the attenuation of light via different mechanisms (explained in section *1.10 Short Wavelength SD-OCT and Active Eye Tracking*). Specifically, this depth depends on 3 factors: the total path length in the material that light has to travel through, the wavelength-dependent proportion of photons scattered per unit length by that material, and the wavelength-dependent proportion of photons absorbed per unit length by that material. Only photons that scatter back to the OCT detector, which are also affected by attenuation and absorbance (double pass), can contribute to the OCT signal. Thus, the transmittance of light through a thick material can be high in poorly absorptive and scattering material (e.g. the vitreous). Vice-versa, a thin material with strong absorptive and/or scattering properties (e.g. the RPE) can greatly attenuate light passing through. Therefore, short wavelength OCT should be less optimal for imaging through scattering tissues like the RPE and choroid.[20,45]

However, a recent study reported on the ability of a short wavelength OCT Angiography device to detect abnormal vasculature in a series of eyes with large pigment epithelial detachments (PEDs), a retinal signature that extends the optical path length in the sub-retinal tissue. Even though the majority of eyes had large PEDs (>0.1mm minimum height), the SD-OCT angiography device showed a sensitivity of 98% in detecting abnormal flow within the PED, when cross-sectional rather than en face OCTA images were assessed.[46] The results of this study suggest that shorter wavelength OCT devices are able to provide images with the clinically relevant information required to make a diagnostic decision, even in ocular conditions that result in thickened retinas.

In terms of choroidal penetration, studies show that long wavelength OCT provides better visibility of the sub-foveal choroidal-scleralinterface (CSI) as compared to short wavelength OCT [21,47–51] Other studies have graded the penetration depth as directly linked with clinically relevant findings (i.e. the depth at which anatomical detail can still be resolved) and concluded that both systems performed equally, although the visibility and contrast of the CSI and choroidal vascular detail was superior on short wavelength OCT images using EDI mode.[52] EDI SD-OCT is useful even in cases with pachychoroid disease, as can be seen in the image comparison of different OCT devices in **Figure 7**.

Both OCT technologies provide similar performance for visualization of relevant diagnostic features of the retina in eyes with polypoidal choroidal vasculopathy, although short wavelength OCT (without using EDI) shows relatively less visibility of the ellipsoid zone and the CSI.[53]

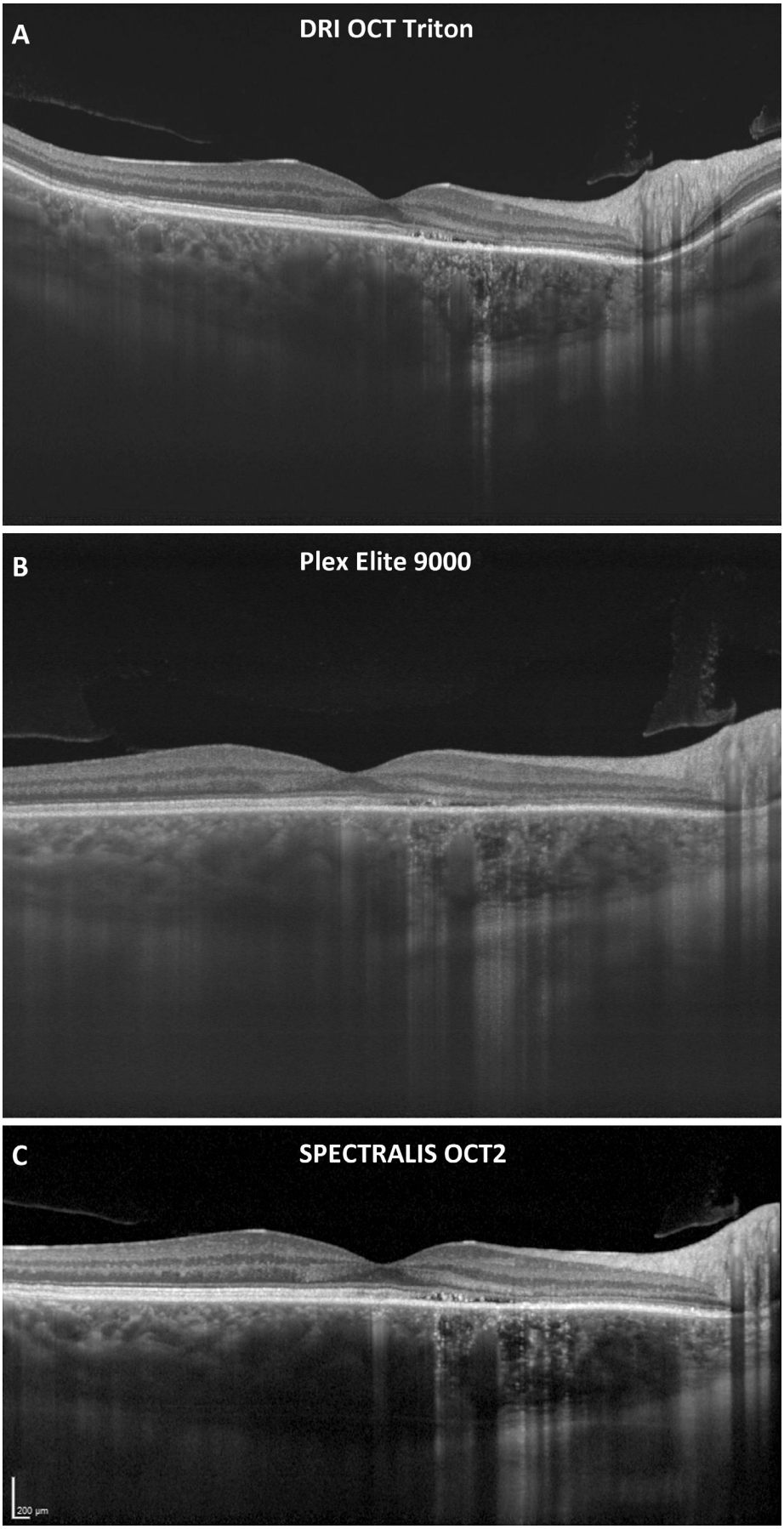

Figure 7. *Comparison of visibility of the choroidal-scleral-interface on images acquired using commercial SS-OCT and SD-OCT devices in a patient with pachychoroid disease (central serous chorioretinopathy).* ***(A)*** *Averaged B-scan (n=128) with DRI OCT Triton SS-OCT device without Dynamic Focusing;* ***(B)*** *Averaged B-scan (n=100) with the Plex Elite 9000 device using EDI-mode;* ***(C)*** *Averaged B-scan (n=100) with SPECTRALIS SD-OCT with OCT2 Module using EDI-mode. The choroidal-scleral-interface is visible on images derived from all three devices.*

A few studies have shown that larger and confluent soft drusen in AMD are spatially correlated with greater losses of OCTA signal in the choriocapillaris using short wavelength OCTA relative to long wavelength OCTA,[54,55] and in most drusen (82.4%) ambiguity remained regarding the absence of flow because structural OCT images also showed loss of signal.[54]

In cases with central serous chorioretinopathy, larger volumes of serous fluid were correlated with proportionately greater losses in OCT signal from the choroid in short wavelength OCT angiography images compared with long wavelength OCT Angiography images.[56] These findings are likely caused by the extended optical path length through the serous fluid, leading to relatively more light scattering and greater loss of OCT sensitivity in deeper choroidal layers on the short wavelength SD-OCT images compared with long wavelength SS-OCT images (section *1.3 Image Depth Range and Signal Roll-Off*). However, the authors' recommendation to use long wavelength SS-OCT to increase the diagnostic accuracy in these cases (especially with large amounts of central serous fluid) is not directly supported by the study results. In another study, although long wavelength SS-OCT Angiography images showed better signal in the evaluation of pigmented lesions such as the microvasculature of melanomas (regardless of tumor size),[57] the authors concluded that the clinical implications of these findings are unclear and that studying the tumor vasculature does not affect the diagnosis of these lesions.[57–62]

1.9 Visibility of Ocular Structures in Eyes that Require an Unusually Long Imaging Depth Range

Long wavelength SS-OCT devices provide axial imaging ranges of 2.6–3 mm [63,64] for posterior segment imaging as compared to short wavelength SD-OCT devices that offer axial imaging ranges of 1.9–2.6 mm. The difference in image depth range can present with clinically relevant findings for posterior segment imaging of eyes with high myopia, as the highly curved retinal surface may be difficult to visualize entirely in a single image. Capturing OCT scans in a wider field than the standard 30° field of view is possible with both SS-OCT and SD-OCT devices

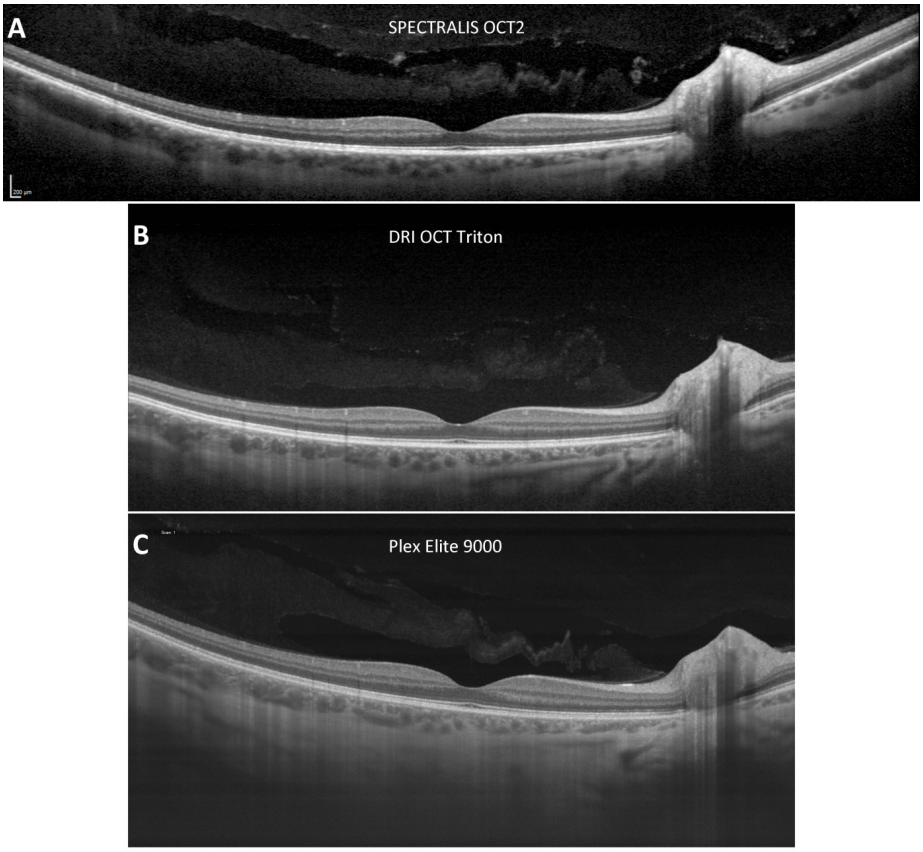

Figure 8. *Comparison of widefield OCT images acquired in volume scans using SS-OCT devices and SPECTRALIS SD-OCT with OCT2 Module.* ***(A)*** *SPECTRALIS OCT2 Module with widefield objective (16.5 mm),* ***(B)*** *Topcon DRI OCT Triton B-scan (12 mm),* ***(C)*** *Zeiss Plex Elite 9000 B-scan (12 mm). SPECTRALIS OCT with widefield lens currently allows the capture of 37.5% wider OCT volume scans.*

(**Figure 8**). The visualization of the retina beyond the posterior pole is facilitated by this capability, while choosing different fixation positions for the patient can help to document the retinal status at larger foveal eccentricities. However, unlike currently available SS-OCT devices, visualizing the wider periphery with SPECTRALIS SD-OCT has the key advantage of a panning camera head to provide the necessary flexibility to reach the far periphery retina. The panning camera head and widefield OCT capability has proven to be a powerful combination, enabling the detection of potentially sight-threatening vitreoretinal pathologies in the mid- to far retinal periphery.[65]

While several studies have indicated that a long wavelength SS-OCT device is able to better visualize some retinal structures in eyes that require an unusually long image depth range (i.e.vitreous imaging, very high myopia, staphylomas), none of the differences are considered clinically significant. Only one small case series (8 eyes) concluded that SS-OCT provides better visualization of the retinal layers in eyes with pathologic myopia compared to SPECTRALIS SD-OCT. However, this difference was not seen in the RPE and sclera.[66] To the best of our knowledge, these results have not been confirmed in larger case series. Visualizing the entire extent of staphylomas in cases with pathologic myopia was possible in 98 out of 100 eyes, and required an SS-OCT system with a 23 mm scan width and a depth range of 5 mm.[67] Another study reported that a 6 mm depth range is required when acquiring 80° (24 mm) widefield SS-OCT images in a single shot, and that this depth range allows for easy capture of images in highly myopic eyes with a limited refractive error of -10 D.[68] In the context of vitreous imaging, the posterior pre-cortical vitreous pockets could be visualized partially with SD-OCT with an additional positive focus shift (depth range of OCT ~1.8 mm),[69–72] whereas its entire structure could be visualized with SS-OCT (depth range, 2.3 mm).[22,73–75]

1.10 Short Wavelength SD-OCT and Active Eye Tracking

In addition to the OCT device's optical set up, technical components, and source spectrum, the tissue properties also determine the level of contrast that can be achieved. Light can be attenuated at surfaces and interfaces with different optical properties, for example a different refractive index. Photons can be absorbed, scattered in a random direction, or can keep following the same path ('transmitted'). Light that is scattered back to the OCT detector is backscattered or 'reflected'. At an optical interface with a difference in refractive index, longer wavelengths of light will have a greater tendency to scatter in the forward direction than light of shorter wavelength, leading to more light penetration through tissue but also to the measurement of less reflectance within the same tissue (**Figure 9**).

To test whether this conjecture applies to OCT imaging, de Boer et al. investigated the intrinsic relative contrast between retinal layers imaged with the same SS-OCT device but using two different light sources – one centered at 845 nm and one at 1060 nm.[45] The results are shown in **Table 1**. A positive value as contrast (in dB) means that the upper layer is more reflective than the lower. Most of the inner retinal layer boundaries showed more contrast using the shorter wavelength, whereas the contrast of outer retinal boundaries tends to be stronger using the longer wavelength (1060 nm). Of note, the contrast between the GCL and IPL was only 0.33 decibels (7.9% difference) with the long wavelength light source as compared to 0.8 decibels (20.2%) using the short wavelength light source. The authors argued that this difference may contribute to less accurate and precise automated segmentation of these retinal boundaries when using long wavelength light sources. Another study compared different SD-OCT devices with comparable axial resolutions,[33] operating with either a long wavelength (1040 nm) or short wavelength (850 nm) and found images obtained with the long wavelength device to generate more variable results when applying the same third-party layer segmentation software optimized for short wavelength SD-OCT images. Therefore, it should be noted that long wavelength

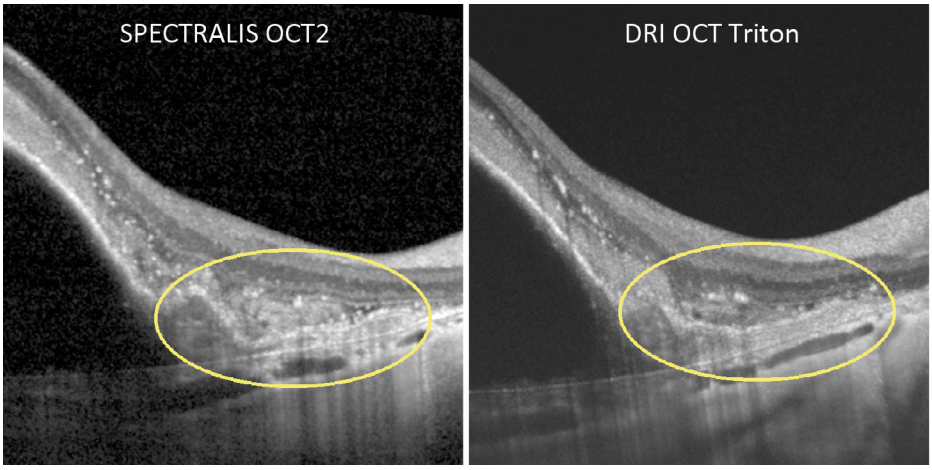

Figure 9. *Comparison of image resolution between SPECTRALIS SD-OCT (left) and a commercial SS-OCT device (right) in a patient with pigment epithelial detachment. For both instruments, image averaging has been applied although the number of images averaged is not equal. Upon close inspection of the figure, more anatomic detail of the polyp lesion in the encircled area can be appreciated on the SD-OCT image, especially with regard to the differentiation and recognition of specific layers based on differences in reflectivity of the tissues.*

OCT images show substantially relevant differences in contrast between the individual layers, which may have clinically relevant implications.[33]

As discussed earlier (section *1.5 Techniques to Enhance Image Contrast and Signal-to-Noise Ratio*), in addition to the implementation of a relatively short wavelength light source that is optimized for retinal imaging, all imaging modalities of SPECTRALIS benefit from TruTrack Active Eye Tracking. This feature reduces random background noise, allowing for greatly enhanced image contrast and better appreciation of the image resolution. When applied to OCT images, not only does Noise Reduction augment the level of anatomic detail discernible by the eye, it also facilitates the precision of segmentation algorithms, especially for retinal layers with poor intrinsic contrast (i.e. the GCL – IPL boundary). This aspect is discussed in section *1.7 (Visibility of Retinal Structures*). Although TruTrack and Automatic Real-Time (ART) averaging can be used for all SPECTRALIS OCT scanning protocols, a similar level of functionality is not offered on most other commercial SD-OCT and SS-OCT devices.

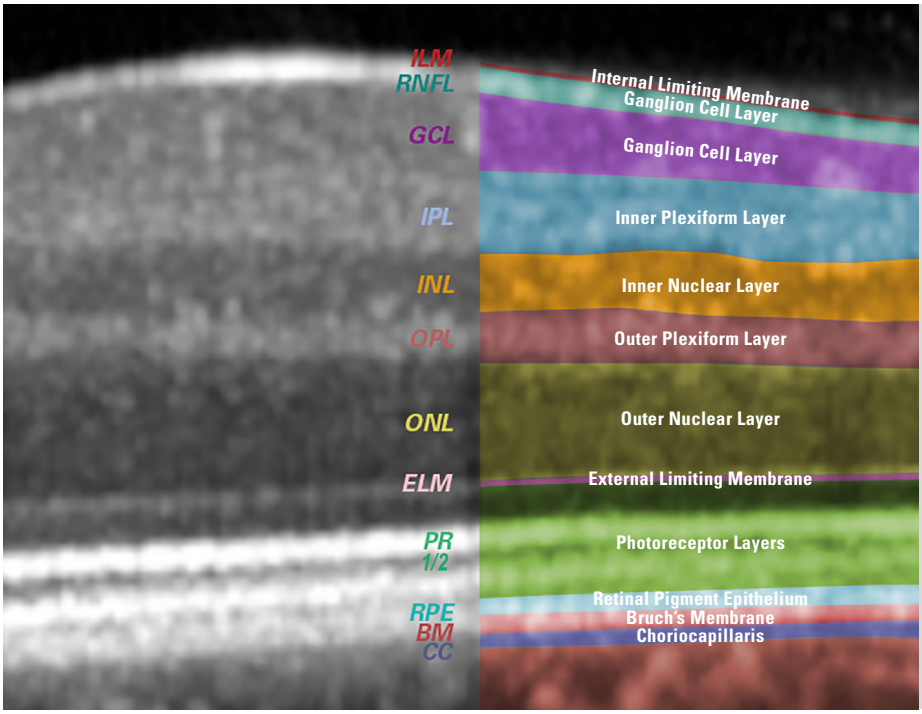

845 nm	1060 nm	Boundary
8.24	6.05	RNFL – GCL
-0.8	-0.33	GCL – IPL
4.03	4.17	IPL – INL
-2.68	-2.89	INL – OPL
5.14	4.42	OPL – ONL
-15.42	-16.06	ONL – EZ
-4.66	-5.83	EZ – Upper RPE
12.68	11.37	Lower RPE – Choroid

Table 1. *The relative contrast or backscattered intensity difference between adjacent retinal layers for 845 and 1060 nm in decibel. A positive value in contrast means that the upper layer is more reflective than the lower.*

LONG WAVELENGTH SS-OCT FOR IMAGING OF THE ANTERIOR SEGMENT

Since commercial SS-OCT devices for anterior segment imaging have been introduced more recently, scientific evidence from direct comparisons between SS-OCT and SD-OCT devices for this application is limited. The absence of vitreous absorption, which is a key contributing factor to signal attenuation of long wavelength light sources for posterior segment imaging, allows for good backscattering from tissue and thus provides the opportunity for high SNR images of deeper anterior segment structures. A long wavelength light source (see section *1.10 Short Wavelength SD-OCT and Active Eye Tracking*) also offers increased image penetration while the Swept-Source technology allows for reduced signal roll-off along a large depth range. The combination of these advantages results in optimized image acquisition of all anterior segment structures. Since the average thickness of the cornea is 500 µm,[76] the anterior chamber depth is 3 mm (range, 1.5 - 4 mm), and the lens thickness varies between 4 to 6 mm, depending on age, it is necessary to acquire high-contrast and high SNR images along this depth range of 10 mm or longer to visualize the entire anterior segment.

Similar to OCT imaging of the posterior segment, differences in the light source wavelength result in relative clinical benefits and limitations. Therefore, short wavelength SD-OCT or long wavelength SS-OCT may offer different applications in the visualization of specific structures in the anterior segment (**Figure 10**).

In addition, details of the anterior chamber angle and iris can be visualized, helping in the diagnosis, treatment, and follow-up of closed-angle glaucoma, for example.

While the SPECTRALIS OCT ASM images offer valuable information related to the cornea, anterior chamber and lens anatomy, the limited image depth range of 1.9 mm prevents the capture of the entire anterior segment within one acquisition. Furthermore, the relatively short wavelength light source results in a lower light penetration through highly scattering tissues such as the sclera and limbus (**Figure 10C and 10D**).[77]

On the other hand, ANTERION® SS-OCT utilizes a 1300 nm light source to offer an axial resolution of less than 10 µm, a lateral scan angle of up to 16.5 mm wide, and a scan depth range of 14 ± 0.5 mm. The long wavelength SS-OCT ANTERION images allow for evaluation of the entire anterior segment, with the advent of being able to visualize all structures of interest in one image.

The high-contrast images are able to detect changes in the corneal anatomy and structure, such as Descemet's membrane detachments, and are ideal for the evaluation of corneal transplants. The visualization of the anterior and posterior surfaces of the lens, together with the anterior chamber, offers clinically relevant information for cataract surgical planning and evaluation. The ability to acquire high-contrast and high-resolution images of the entire anterior chamber allows not just for qualitative visualization of the anterior chamber architecture, but also for quantitative assessment of several clinically relevant parameters such as anterior chamber angle,[78] anterior chamber depth and volume, spur-to-spur distance, and lens vault. The ability to measure such parameters while being able to visualize the entire anterior segment at various angles is useful as a complementary tool to gonioscopy, with the additional benefit of allowing better documentation and OCT being a non-contact technique.[79] Thus, considering the technical specifications of SS-OCT technology combined with a long wavelength light source and the potential advantages that this combination offers (described in section *1.3 Image Depth Range and Signal Roll-Off*), long wavelength SS-OCT is the optimal device configuration for comprehensive anterior segment imaging.

CONCLUSIONS

The main advantages and limitations of the two Fourier-Domain OCT technologies, SS-OCT and SD-OCT, have been reviewed. SD-OCT employs a super-luminescent diode and a line-scan camera, whereas SS-OCT (introduced shortly after the commercial implementation of Spectral-Domain OCT technology) uses a frequency-swept laser and photodiode to analyze light returning from the sample. Swept-Source OCT technology was thought to offer potential acquisition speed advantages, however, the advancement of SD-OCT technology has led to the development of commercial SD-OCT devices with faster acquisition speed than available SS-OCT devices. In fact, the fastest OCT device in the market uses SD-OCT technology (250k A-scans/s).[14]

Furthermore, SS-OCT technology typically includes light sources with longer center wavelengths than those implemented in SD-OCT devices. In order for the longer wavelength SS-OCT devices to achieve similar axial resolution relative to the shorter wavelength SD-OCT devices, they have employed light sources with broader spectral bandwidth. Improving the axial resolution of SS-OCT devices is physically limited by restrictions on broader spectral bandwidth combined with the water absorption limitations for imaging the posterior pole at these longer wavelengths. These limitations are not as applicable to shorter wavelength SD-OCT devices.

The sensitivity of SD-OCT and SS-OCT devices depends on laser power.[12] While the employment of a longer wavelength with SS-OCT allows for the use of more laser power, the signal light suffers more attenuation by water in the vitreous. The signal-to-noise ratio of retinal tissue measured in-vivo is nearly the same regardless of wavelength,[45] suggesting that the higher achievable sensitivity of SS-OCT is not clinically meaningful in-vivo. A tradeoff between signal roll-off and the axial scan range is applicable to both OCT technologies but the difference in roll-off between the state-of-the-art commercial systems is negligible. Although longer wavelength light tends to penetrate deeper into biological tissues, it does so

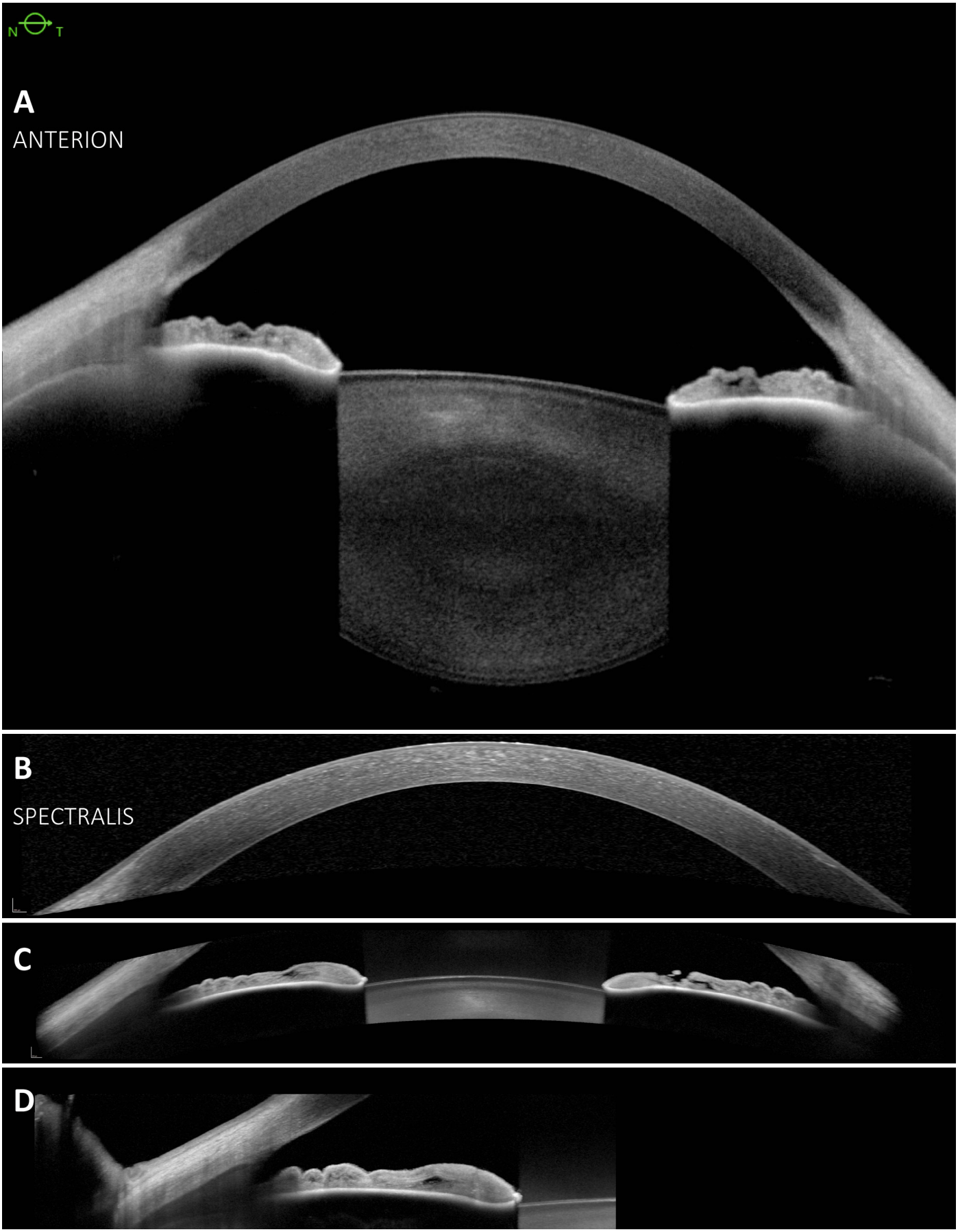

Figure 10. *Anterior segment of a healthy eye imaged with both SS-OCT and SD-OCT technologies.* ***(A)*** *ANTERION* SS-OCT allows for the capture of high-contrast and high-resolution images of the entire anterior segment (cornea, anterior chamber, iris, and lens). The SPECTRALIS SD-OCT Anterior Segment Module (ASM) images may provide more structural details due to the higher axial resolution. The following structures can be compared side by side:* ***(A)*** *entire anterior segment using ANTERION,* ***(B)*** *cornea using SPECTRALIS ASM,* ***(C)*** *iris and anterior chamber angles using SPECTRALIS ASM, and* ***(D)*** *zoomed anterior chamber angle using SPECTRALIS ASM.*

**ANTERION is currently not for sale in the USA.*

at the cost of reduced intrinsic contrast between different tissues. This principle has important implications in retinal imaging, considering the near-optical transparency of retinal structures.

Heidelberg Engineering SPECTRALIS is the only SD-OCT device that combines OCT with cSLO multimodal imaging and TruTrack Active Eye Tracking as one of its core technologies. TruTrack allows for enhanced SNR and precise follow-up scanning at the same retinal location. These enhancements enable clinicians to more accurately and precisely delineate intra-retinal layers (**Figure 6**) such as the GCL and IPL, and to accurately monitor small changes, making the diagnosis and management of certain diseases such as glaucoma reliable over time.

The clinical relevance for the use of a longer wavelength light source combined with SS-OCT technology to better visualize certain posterior segment structures remains unknown. For example, in some limited occurrences of macular hole and retinal detachment surgery, where the vitreous cavity is filled with gas, the use of longer wavelength SS-OCT devices may allow for better visualization of the hole. Nevertheless, shorter wavelength SD-OCT devices are also able to discern these holes albeit with less clarity. However, longer wavelength SS-OCT technology provides the advantage of a longer imaging depth with less signal roll-off along this depth, which may be advantageous for widefield imaging where the curvature of the eye leads to the need of a longer depth imaging range. In order to mitigate this potential limitation, the SPECTRALIS SD-OCT offers a panning camera head that provides the needed flexibility to acquire B-scans even in the far retinal periphery. In addition, the TruTrack and Automatic Real-Time (ART) averaging are available in all scanning protocols on the SPECTRALIS OCT, giving the opportunity to increase the quality of the images as needed.

Short wavelength SD-OCT technology and long wavelength SS-OCT technology both pose unique advantages and limitations for imaging of the anterior segment of the eye. The use of a longer wavelength light source offers a longer depth imaging range in scattering tissues. The better signal roll-off of SS-OCT technology relative to SD-OCT technology is especially applicable to longer axial imaging ranges, thereby being optimal for the acquisition of high-contrast and high-resolution images of the entire anterior segment in one image. The use of a longer wavelength is also advantageous for anterior segment imaging, as the water absorption limitation that is applicable to posterior segment imaging is significantly marginalized when imaging the anterior segment. While the Anterior Segment Module (ASM) of SPECTRALIS SD-OCT provides high-contrast and high-resolution images of anterior segment structures within a limited depth range, the ANTERION SS-OCT (1300 nm light source) offers the ability to quickly acquire images of the entire anterior segment. The ability to image the anterior segment with high-contrast and high-resolution in one image facilitates the clinical evaluation and measurement of structures needed for detection and management of anterior segment abnormalities, as well as for refractive surgery.

While SS-OCT technology continues to evolve and has yet to show clear clinically relevant advantages relative to SD-OCT technology, Heidelberg Engineering is confident that SS-OCT technology will play a key role in the advancement of high-resolution ocular imaging in the future. Based on the current limitations and advantages of SS-OCT technology, the implementation of a longer wavelength SS-OCT device is optimal for penetrating the structures in the anterior segment. The ANTERION is an SS-OCT device optimized to combine all relevant anterior segment examinations in one modular, upgradeable platform. With the commercial release of ANTERION, Heidelberg Engineering's optimization of SS-OCT technology for anterior segment imaging and of SD-OCT technology for retinal imaging will deliver images that empower clinicians to make confident diagnostic decisions, disease management, surgical planning and follow-up to improve patient care.

References

1. Huang D, Swanson EA, Lin CP, et al. Optical coherence tomography. Science. 1991;254(5035):1178-81. doi: 10.1126/science.1957169.
2. Fercher AC, Hitzenberger CK, Kamp G, et al. Measurement of intraocular distances by backscattering spectral interferometry. Opt. Commun. 1995;117(1-2):43-8. doi:10.1016/0030-4018(95)00119-S.
3. Optovue RTVue 510(K) Premarket Notification; 2006. https://www.accessdata.fda.gov/cdrh_docs/pdf6/K062552.pdf. Accessed November 19, 2018.
4. de Boer JF, Cense B, Park BH, et al. Improved signal-to-noise ratio in spectral domain compared with time domain optical coherence tomography. Opt Lett. 2003;28(21):2067-9. doi:10.1364/OL.28.002067.
5. Leitgeb R, Hitzenberger C, Fercher A. Performance of Fourier domain vs. time domain optical coherence tomography. Opt Express. 2003;11(8):889-94. doi:10.1364/OE.11.000889.
6. Chinn SR, Swanson EA, Fujimoto JG. Optical coherence tomography using a frequency-tunable optical source. Opt Lett. 1997;22(5):340-2. doi:10.1364/OL.22.000340.
7. Golubovic B, Bouma BE, Tearney GJ, et al. Optical frequency-domain reflectometry using rapid wavelength tuning of a Cr4+:forsterite laser. Opt Lett. 1997;22(22):1704-6. doi:10.1364/OL.22.001704.
8. Lexer F, Hitzenberger CK, Fercher AF, et al. Wavelengthtuning interferometry of intraocular distances. Appl Opt. 1997;36(25):6548-53. doi:10.1364/AO.36.006548.
9. Hiratsuka H, Kido E, Yoshimura T. Simultaneous measurements of three-dimensional reflectivity distributions in scattering media based on optical frequency-domain reflectometry. Opt Lett. 1998;23(18):1420-2. doi:10.1364/OL.23.001420.
10. Haberland UH, Blazek V, Schmitt HJ. Chirp optical coherence tomography of layered scattering media. J Biomed Opt. 1998;3(3):259-66. doi:10.1117/1.429889.
11. He Z, Hotate K. Synthesized optical coherence tomography for imaging of scattering objects by use of a stepwise frequency-modulated tunable laser diode. Opt Lett. 1999;24(21):1502-4. doi:10.1364/OL.24.001502.
12. Choma M, Sarunic M, Yang C, et al. Sensitivity advantage of swept source and Fourier domain optical coherence tomography. Opt Express. 2003; 11(18):2183-9. doi:10.1364/OE.11.002183.
13. Topcon Medical Systems to Launch Five New Products at the AAO: DRI OCT-1 Atlantis; 2012. www.topconmedical.com/_assets/cf/downloadFile.cfm?section=news&file=Topcon_Press_Release_topcon-launches-5-new-products-at-aao.pdf. Accessed November 19, 2018.
14. Optopol Technology. Flux - Next generation widefield OCT. http://optopol.com/products/FLUX. Accessed 26th September 2018.
15. Hausler G, Lindner MW. "Coherence radar" and "spectral radar"-new tools for dermatological diagnosis. J Biomed Opt. 1998;3(1):21-31. doi:10.1117/1.429899.
16. Wojtkowski M, Leitgeb R, Kowalczyk A, et al. In vivo human retinal imaging by Fourier domain optical coherence tomography. J Biomed Opt. 2002;7(3): 457-63. doi:10.1117/1.1482379.
17. Cense B, Nassif N, Chen T, et al. Ultrahigh-resolution high-speed retinal imaging using spectraldomain optical coherence tomography. Opt Express. 2004;12(11):2435-47. doi:10.1364/OPEX.12.002435.
18. Wojtkowski M, Srinivasan V, Ko T, et al. Ultrahighresolution, high-speed, Fourier domain optical coherence tomography and methods for dispersion compensation. Opt Express. 2004;12(11):2404-22. doi:10.1364/OPEX.12.002404.
19. Spaide RF, Akiba M, Ohno-Matsui K. Evaluation of peripapillary intrachoroidal cavitation with swept source and enhanced depth imaging optical coherence tomography. Retina. 2012;32(6):1037-44. doi:10.1097/IAE.0b013e318242b9c0.
20. Verner-Cole EA, Campbell JP, Hwang TS, et al. Retinal and choroidal imaging with 870-nm spectral domain OCT compared with 1050-nm spectral domain OCT, with and without enhanced depth imaging. Trans. Vis. Sci. Tech. 2014;3(3):3. doi:10.1167/tvst.3.3.3.
21. Barteselli G, Bartsch D, Weinreb RN, et al. Real-time full-depth visualization of posterior ocular structures: Comparison between full-depth imaging spectral domain optical coherence tomography and swept-source optical coherence tomography Retina. 2016;36(6):1153-61.doi:10.1097/IAE.0000000000000842.
22. Itakura H, Kishi S, Li D, Akiyama H. Observation of posterior precortical vitreous pocket using sweptsource optical coherence tomography. Invest Ophthalmol Vis Sci. 2013;54(5):3102-7. doi:10.1167/iovs.13-11769.
23. Itakura H, Kishi S. Aging changes of vitreomacular interface. Retina. 2011;31(7):1400-4. doi:10.1097/IAE.0b013e318206cb43.
24. Pizer SM, Amburn EP, Austin JD, et al. Adaptive histogram equalization and its variations. Comput Vis Graphics Imaging Process. 1987;39:355-68. doi: 10.1016/S0734-189X(87)80186-X.
25. Liu JJ, Witkin AJ, Adhi M, et al. Enhanced vitreous imaging in healthy eyes using swept source optical coherence tomography. PloS one. 2014;9(7):e102950. doi:10.1371/journal.pone.0102950.
26. Li D, Kishi S, Itakura H, et al. Posterior precortical vitreous pockets and connecting channels in children on swept-source optical coherence tomography. Invest Ophthalmol Vis Sci. 2014;55(4):2412-6. doi:10.1167/iovs.14-13967.
27. Lavinsky F, Lavinsky D. Novel perspectives on sweptsource optical coherence tomography. Int J Retin Vitr. 2016;2:25. doi:10.1186/s40942-016-0050-y.

References

28. Lee SY, Bae HW, Kwon HJ, et al. Repeatability and agreement of swept source and spectral domain optical coherence tomography evaluations of thickness sectors in normal eyes. J Glaucoma. 2017;26(2):e46-e53. doi:10.1097/IJG.0000000000000536.
29. Lee SY, Bae HW, Seong GJ, et al. Diagnostic ability of swept-Source and spectral domain optical coherence tomography for glaucoma. Yonsei Med J. 2018;59(7):887-96. doi:10.3349/ymj.2018.59.7.887.
30. Ha A, Lee SH, Lee EJ, et al. Retinal nerve fiber layer thickness measurement comparison using spectral domain and swept source optical coherence tomography. Korean J Ophthalmol. 2016;30(2):140-7. doi:10.3341/kjo.2016.30.2.140.
31. Lee KM, Lee EJ, Kim T, et al. Comparison of the abilities of SD-OCT and SS-OCT in evaluating the thickness of the macular inner retinal layer for glaucoma diagnosis. PloS one. 2016;11(1):e0147964. doi:10.1371/journal.pone.0147964.
32. Yang Z, Tatham AJ, Weinreb RN, et al. Diagnostic ability of macular ganglion cell inner plexiform layer measurements in glaucoma using swept source and spectral domain optical coherence tomography. PloS one. 2015;10(5):e0125957. doi:10.1371/journal.pone.0125957.
33. Terry L, Cassels N, Lu K, et al. Automated retinal layer segmentation using spectral domain optical coherence tomography: Evaluation of inter-session repeatability and agreement between devices. PloS one. 2016;11(9):e0162001. doi:10.1371/journal.pone.0162001.
34. Quigley HA, McKinnon SJ, Zack DJ, et al. Retrograde axonal transport of BDNF in retinal ganglion cells is blocked by acute IOP elevation in rats. Invest Ophthalmol Vis Sci. 2000;41(11):3460-6.
35. Mwanza J, Oakley JD, Budenz DL, Chang RT, Knight OJ, Feuer WJ. Macular ganglion cell-inner plexiform layer: automated detection and thickness reproducibility with spectral domain-optical coherence tomography in glaucoma. Invest Ophthalmol Vis Sci. 2011;52(11):8323-9. doi:10.1167/iovs.11-7962.
36 Chien JL, Ghassibi MP, Patthanathamrongkasem T, et al. Glaucoma diagnostic capability of global and regional measurements of isolated ganglion cell layer and inner plexiform layer. J Glaucoma. 2017;26(3):208-15. doi:10.1097/IJG.0000000000000572.
37. Lin P, Chang H, Lin J, et al. Analysis of peripapillary retinal nerve fiber layer and inner macular layers by spectral domain optical coherence tomography for detection of early glaucoma. Int J Ophthalmol. 2018;11(7):1163-72. doi:10.18240/ijo.2018.07.15.
38. Springelkamp H, Lee K, Wolfs, et al. Population-based evaluation of retinal nerve fiber layer, retinal ganglion cell layer, and inner plexiform layer as a diagnostic tool for glaucoma. Invest Ophthalmol Vis Sci. 2014;55(12):8428-38. doi:10.1167/iovs.14-15506.
39. Fry LE, Fahy E, Chrysostomou V, et al. The coma in glaucoma: Retinal ganglion cell dysfunction and recovery. Prog Retin Eye Res. 2018;65:77-92. doi:10.1016/j.preteyeres.2018.04.001.
40. Curcio CA, Allen KA. Topography of ganglion cells in human retina. J Comp Neurol. 1990;300(1):5-25. doi:10.1002/cne.903000103.
41. Hood DC, Raza AS, de Moraes, et al. Glaucomatous damage of the macula. Prog Retin Eye Res. 2013;32:1-21. doi:10.1016/j.preteyeres.2012.08.003.
42. Kim EK, Park HL, Park CK. Segmented inner plexiform layer thickness as a potential biomarker to evaluate open-angle glaucoma: Dendritic degeneration of ' retinal ganglion cell. PloS one. 2017;12(8):e0182404. doi:10.1371/journal.pone.0182404.
43. Povazay B, Hermann B, Unterhuber A, et al. Three-dimensional optical coherence tomography at 1050 nm versus 800 nm in retinal pathologies: Enhanced performance and choroidal penetration in cataract patients. J Biomed Opt. 2007;12(4):041211. doi:10.1117/1.2773728.
44. Ahn SJ, Park SH, Lee BR. Visualization of the macula in gas-filled eyes: Spectral domain optical coherence tomography versus swept source optical coherence tomography. Retina. 2018;38(3):480-9. doi:10.1097/IAE.0000000000001560.
45. Chen Y, Burnes DL, Bruin M de, et al. Three-dimensional pointwise comparison of human retinal optical property at 845 and 1060 nm using optical frequency domain imaging. J Biomed Opt. 2009;14(2):024016. doi:10.1117/1.3119103.
46. Tan, Anna C S, Freund KB, et al. Imaging of pigment epithelial detachments with optical coherence tomography angiography. Retina. 2017. doi:10.1097/IAE.0000000000002016.
47. Adhi M, Liu JJ, Qavi AH, et al. Enhanced visualization of the choroido-scleral interface using swept-source OCT. Ophthalmic Surg Lasers Imaging Retina. 2013;44(6 Suppl):S40-2. doi:10.3928/23258160-20131101-08.
48. Adhi M, Liu JJ, Qavi AH, et al. Choroidal analysis in healthy eyes using swept-source optical coherence tomography compared to spectral domain optical coherence tomography. Am J Ophthalmol. 2014;157(6):1272-81.e1. doi:10.1016/j.ajo.2014.02.034.
49. Park HL, Shin H, Park CK. Imaging the posterior segment of the eye using swept-source optical coherence tomography in myopic glaucoma eyes: Comparison with enhanced-depth imaging. Am J Ophthalmol. 2014;157(3):550-557. doi:10.1016/j.ajo.2013.11.008.
50. Tan, Colin S H, Ngo WK, et al. Comparison of choroidal thicknesses using swept source and spectral domain optical coherence tomography in diseased and normal eyes. Br J Ophthalmol. 2015;99(3):354-8. doi:10.1136/bjophthalmol-2014-305331.
51. Mrejen S, Spaide RF. Optical coherence tomography: imaging of the choroid and beyond. Surv Ophthalmol. 2013;58(5) :387-429. doi:10.1016/ j.survophthal. 2012.12.001.
52. Waldstein SM, Faatz H, Szimacsek M, et al. Comparison of penetration depth in choroidal imaging using swept source vs spectral domain optical coherence tomography. Eye (Lond). 2015;29(3):409-15. doi:10.1038/eye.2014.319.
53. Ting, Daniel S W, Cheung, Gemmy C M, Lim LS, Yeo, Ian Y S. Comparison of swept source optical coherence tomography and spectral domain optical coherence tomography in polypoidal choroidal vasculopathy. Clin Experiment Ophthalmol. 2015;43(9):815-9. doi:10.1111/ceo.12580.

References

54. Lane M, Moult EM, Novais EA, et al. Visualizing the choriocapillaris under drusen: Comparing 1050-nm swept-source versus 840-nm spectral domain optical coherence tomography angiography. Invest Ophthalmol Vis Sci. 2016;57(9):OCT585-90. doi:10.1167/iovs.15-18915.

55. Chatziralli I, Theodossiadis G, Panagiotidis D, et al. Choriocapillaris vascular density changes in patients with drusen: Cross-sectional study based on optical coherence tomography angiography findings. Ophthalmol Ther. 2018;7(1):101-7. doi:10.1007/s40123-018-0119-9.

56. Wang F, Zhang Q, Deegan AJ, et al. Comparing imaging capabilities of spectral domain and swept source optical coherence tomography angiography in healthy subjects and central serous retinopathy. Eye Vis (Lond). 2018;5:19. doi:10.1186/s40662-018-0113-2.

57. Pellegrini M, Corvi F, Invernizzi A, et al. Swept-source optical coherence tomography angiography in choroidal melanoma: An analysis of 22 consecutive cases. Retina. 2018. doi:10.1097/IAE.0000000000002205.

58. Edwards WC, Layden WE, Macdonald R. Fluorescein angiography of malignant melanoma of the choroid. Am J Ophthalmol. 1969;68(5):797-808. doi:10.1016/0002-9394(69)94571-1.

59. Pettit TH, Barton A, Foos RY, et al. Fluorescein angiography of choroidal melanomas. Arch Ophthalmol. 1970;83(1):27-38. doi:10.1001/archopht.1970.00990030029006

60. Mueller AJ, Freeman WR, Folberg R, et al. Evaluation of microvascularization pattern visibility in human choroidal melanomas: comparison of confocal fluorescein with indocyanine green angiography. Graefes Arch. Clin. Exp. Ophthalmol. 1999;237(6):448-56. doi:10.1007/s004170050260.

61. Schaller UC, Mueller AJ, Bartsch DU, et al. Choroidal melanoma microcirculation with confocal indocyanine green angiography before and 1 year after radiation brachytherapy. Retina. 2000;20(6):627-32. doi:10.1097/00006982-200006000-00008.

62. Mueller AJ, Bartsch DU, Folberg R, et al. Imaging the microvasculature of choroidal melanomas with confocal indocyanine green scanning laser ophthalmoscopy. Arch Ophthalmol. 1998;116(1):31-9. doi:10.1001/archopht.116.1.31.

63. Topcon Europe Medical B.V. DRI OCT Triton, Swept source OCT: Product description. http://www.topconmedical.eu/eu/products/382-dri-oct-triton-sweptsource-oct.html.

64. Carl Zeiss Meditec, Inc. Plex Elite 9000 OCT Angiography: Product description:www.zeiss.com/content/dam/Meditec/downloads/pdf/ari-networkdownload/plex-elite-brochure_en_31_020_0001v_us_31_020_0001v.pdf.

65. Cereda MG, Corvi F, Cozzi M, et al. Optical coherence tomography 2: Diagnostic tool to study peripheral vitreoretinal pathologies. Retina. 2017. doi:10.1097/IAE.0000000000001953.

66. Lim LS, Cheung G, Lee SY. Comparison of spectral domain and swept-source optical coherence tomography in pathological myopia. Eye (Lond). 2014;28(4):488-91. doi:10.1038/eye.2013.308.

67. Shinohara K, Shimada N, Moriyama M, et al. Posterior staphylomas in pathologic myopia imaged by widefield optical coherence tomography. Invest Ophthalmol Vis Sci. 2017;58(9):3750-8. doi:10.1167/iovs.17-22319.

68. 80 degree field of view swept-source optical coherence tomography. [Bello, Doug Howard1, Muzammil A. Arain, Atoosa Moghimi, Jochen Straub, Tilman Schmoll]; Association for Research and Vision in Ophthalmology Annual Meeting 2018, Abstract number 1527.

69. Spaide RF. Measurement of the posterior precortical vitreous pocket in fellow eyes with posterior vitreous detachment and macular holes. Retina. 2003;23(4): 481-5. doi:10.1097/00006982-200308000-00006

70. Johnson MW. Posterior vitreous detachment: evolution and complications of its early stages. Am J Ophthalmol. 2010;149(3):371-82.e1. doi:10.1016/j.ajo.2009.11.022.

71. Mojana F, Kozak I, Oster SF, et al. Observations by spectral domain optical coherence tomography combined with simultaneous scanning laser ophthalmoscopy: imaging of the vitreous. Am J Ophthalmol. 2010;149(4):641-50. doi:10.1016/j.ajo.2009.11.016.

72. Itakura H, Kishi S. Evolution of vitreomacular detachment in healthy subjects. JAMA Ophthalmol. 2013;131(10):1348-52. doi:10.1001/jamaophthalmol.2013.4578.

73. Yokoi T, Toriyama N, Yamane T, et al. Development of a premacular vitreous pocket. JAMA Ophthalmol. 2013;131(8):1095-6. doi:10.1001/jamaophthalmol.2013.240.

74. Itakura H, Kishi S, Li D, et al. Vitreous changes in high myopia observed by swept-source optical coherence tomography. Invest Ophthalmol Vis Sci. 2014;55(3):1447-52. doi:10.1167/iovs.13-13496.

75. Stanga PE, Sala-Puigdollers A, Caputo S, et al. In vivo imaging of cortical vitreous using 1050-nm swept-source deep range imaging optical coherence tomography. Am J Ophthalmol. 2014; 157(2):397-404.e2. doi:10.1016/j.ajo.2013.10.008.

76. American Academy of Ophthalmology. 2016 - 2017 Basic and Clinical Science Course: Fundamentals and Principles of Ophthalmology: American Academy of Ophthalmology; 2016.

77. Shapiro BL, Cortes DE, Chin EK, et al. High-resolution spectral domain anterior segment optical coherence tomography in type 1 Boston keratoprosthesis. Cornea. 2013;32(7):951-5. doi:10.1097/ICO.0b013e318285c8f4.

78. Romkens, Hellen C. S., Beckers, et al. Reproducibility of anterior chamber angle analyses with the sweptsource optical coherence tomography in young, healthy Caucasians. Invest Ophthalmol Vis Sci. 2014;55(6). doi:10.1167/iovs.13-12904.

79. Rigi M, Bell NP, Lee DA, et al. Agreement between gonioscopic examination and swept source Fourier domain anterior segment optical coherence tomography imaging. J Ophthalmol. 2016;2016:1727039.doi:10.1155/2016/1727039.

HEIDELBERG ENGINEERING ACADEMY

Headquarters
Heidelberg Engineering GmbH · Max-Jarecki-Str. 8 · 69115 Heidelberg · Germany
Tel. +49 6221 64630 · Fax +49 6221 646362

AUS
Heidelberg Engineering Pty Ltd · Suite E5, 63 - 85 Turner St · Port Melbourne VIC 3207
Tel. +61 396 392 125 · Fax +61 396 392 127

CH
Heidelberg Engineering GmbH · Schulstrasse 161 · 8105 Regensdorf
Tel. +41 44 888 70 20 · Fax +41 44 888 70 24

FIN
Heidelberg Engineering GmbH · Luomannotko 6 · 02200 Espoo
Tel. +358 505 226 963

UK
Heidelberg Engineering Ltd. · 55 Marlowes · Hemel Hempstead · Hertfordshire HP1 1LE
Tel. +44 1442 502 330 · Fax +44 1442 242 386

USA
Heidelberg Engineering, Inc. · 10 Forge Parkway · Franklin, MA 02038
Tel. +1 508 530 7900 · Fax +1 508 530 7901

www.HeidelbergEngineering.com · Information@HeidelbergEngineering.com

200425-002 GL.AE19 © Heidelberg Engineering GmbH